JOURNAL OF GEOPHYSICAL RESEARCH, VOL. 88, NO. A12, PAGES 10,053–10,058, DECEMBER 1, 1983

A Theoretical Model Study of Observed Correlations Between Whistler Mode Waves and Energetic Electron Precipitation Events in the Magnetosphere

H. C. CHANG AND U. S. INAN

Space, Telecommunications and Radioscience Laboratory, Stanford University

A recently extended test particle computer model of the gyroresonance wave-particle interaction in the magnetosphere is applied to previously reported cases of observed correlations between whistler mode waves and ionospheric responses to particle precipitation. Three different ionospheric effects, namely, X ray bursts, photoemissions, and D region perturbations, all correlated with VLF waves and believed to be caused by precipitated particles, are considered. The precipitation flux level, the pulse shape, and the associated time delays are computed for the parameters relevant to each case and are compared with values deduced from the data. The results demonstrate that the existing theoretical model can be useful for interpreting experimental results of this kind. Furthermore, the model results and observations, used together, provide a basis for additional diagnostics of the various parameters of the cold and energetic particle distributions in the magnetosphere. For example, when applied to the observed photoemission case (Helliwell et al., 1980) the model results imply that the trapped energetic particle distribution function at the time could be modeled as proportional to $E^{-n/2}$ with $n \simeq 3.5$ to 6, where E is the particle energy.

1. INTRODUCTION

One result of whistler mode wave-particle interactions in the magnetosphere is pitch angle scattering by the wave and the resulting precipitation of energetic electrons into the atmosphere. These electrons, when penetrating the lower ionosphere, can cause ionization and conductivity enhancements, heating, and the emission of X rays and light.

Recent experiments have shown an association between isolated bursts of precipitating electrons at middle latitudes ($L < 6$) and whistlers and triggered emissions. The first observed correlation between discrete VLF waves (propagating at $L \simeq 4.2$) and bursts of bremsstrahlung X rays (>30 keV) observed at balloon altitudes was reported by *Rosenberg et al.* [1971]. *Helliwell et al.* [1973] reported correlations between whistlers and perturbations in the intensity of fixed-frequency VLF signals propagating in the nighttime earth-ionosphere waveguide. The observed perturbations were attributed to whistler-induced precipitation of energetic (>30 keV) electrons that cause a transient enhancement of the electron population in the D region and thus perturb VLF propagation in the waveguide. Other related reports include those of *Foster and Rosenberg* [1976], *Rosenberg et al.* [1981], *Lohrey and Kaiser* [1979], *Dingle and Carpenter* [1981], and *Carpenter and LaBelle* [1982]. The work of *Rosenberg et al.* [1981] established a correspondence between VLF chorus at Siple and electron precipitation microbursts at the conjugate Roberval station.

In addition to the X ray and VLF methods, photometric measurements of light emission caused by precipitated electrons have also been employed to explore VLF wave-induced precipitation events. This method provides better spatial resolution of the precipitating particles and is capable of covering the lower range of the electron energies. *Helliwell et al.* [1980] found one-to-one correlations between bursts of $\lambda \simeq 4278$ Å light emissions and quasi-coherent ducted VLF waves during photometric observations at Siple Station, Antarctica. *Doolittle and Carpenter* [1983] reported a case of one-to-one correlations between optical emissions and whistler-induced noise events recorded at Roberval.

All of the above mentioned observations of correlation events were attributed to a cyclotron resonance interaction between energetic electrons and whistler mode wave packets traveling along the earth's magnetic field lines [e.g., *Inan et al.*, 1978]. The interpretation was often based on comparing the measured time lag between the wave and precipitation bursts with the estimated travel times of the wave and the particles from the interaction region to the observation site. The models used have been steadily refined; for example, *Doolittle* [1982] explored the distinction between the effects of scattered particles that mirror in one hemisphere before precipitation and those that precipitate 'directly.' The previous models also revealed features such as arrival time focusing of particles of different energies and included off-equatorial interactions [*Helliwell et al.*, 1980].

The previous studies and models were largely based on analytical formulations of varying complexity. In general, it was not possible to estimate the amplitude or the structure of the precipitation pulse that would be induced by a given wave. The effects of changing frequency or full nonlinear scattering involving relativistic energies were not considered. Although the previous calculations constitute a first-order test of the assumed process of cyclotron resonance interactions, in this paper we apply a test particle computer model of the gyroresonant wave-particle interaction for the purpose of computing the precipitation flux level, pulse shape, and associated time relationships and comparing these with the reported data.

The test particle model has been recently developed and applied to the study of transient particle precipitation induced by short-duration VLF wave pulses propagating along the earth's magnetic field lines [*Inan et al.*, 1978, 1982]. This model has been further extended to cases involving quasi-

Paper number 3A1545.
0148-0227/83/003A-1545$05.00

relativistic particles [*Chang and Inan,* 1983] and coherent waves with slowly varying frequency [*Chang et al.,* 1983]. The model takes into account the travel times of the wave and the particles and computes the wave-induced pitch angle change of a large number of individual resonant test particles in order to infer the perturbations of the distribution function and the transient evolution of the precipitation flux.

In this paper we apply the model to observed correlations reported by *Rosenberg et al.* [1971] and *Helliwell et al.* [1973, 1980].

2. Description of the Model

We consider a VLF wave pulse of finite duration and of either fixed or variable frequency originating in the magnetosphere at 1000 km altitude and at time $t = 0$. The wave packet is assumed to propagate in a whistler mode duct along a specific field line with the wave vector $\mathbf{k} \parallel \mathbf{B}_o$, where $\mathbf{B}_o$ is the static magnetic field. For the background magnetosphere, we use a centered dipole model of the earth's magnetic field and either a diffusive equilibrium model or a collisionless model for the cold plasma distribution.

As the input wave packet propagates along the field line, it interacts with particles for which the resonance condition

$$\omega - \mathbf{k} \cdot \mathbf{v} \simeq \omega_H/\gamma \tag{1}$$

is locally satisfied, where ω is the wave frequency, ω_H is the local electron gyrofrequency, $\mathbf{v}$ is the total velocity of the particle, and $\gamma = (1 - v^2/c^2)^{-1/2}$, c being the velocity of light. For the whistler mode wave ($\omega_H > \omega$), (1) is satisfied for electrons that travel in a direction opposite to that of the wave unless $\omega_H/\gamma < \omega$.

The initial unperturbed particle distribution is represented by an equatorial distribution function $f(E, \alpha)$, where E is the total energy and α is the equatorial pitch angle of the particle, and is taken to be of the form

$$f(E, \alpha) = AE^{-n/2} g(\alpha) \qquad \alpha \geq \alpha^{lc} \tag{2}$$

where A is a constant, $n/2$ is an exponent that can be adjusted to fit observed distributions, $g(\alpha)$ is some function of pitch angle, and α^{lc} is the angular half width of the loss cone. We consider an initially empty loss cone so that $f(E, \alpha) = 0$ for $\alpha < \alpha^{lc}$. For the purpose of comparing with observed distributions conventionally described in terms of the differential energy spectrum in el cm^{-2} s^{-1} sr^{-1} keV^{-1}, the constant A can be related to the differential energy spectrum Φ_E of electrons at a given energy E(keV) and with $\alpha = 90^\circ$ pitch angle as $A = \Phi_E(m^2/mc^2)(\gamma_E{}^5/(\gamma_E{}^2 - 1))E^{n/2}$, where mc^2 is the rest energy of the electron, m is the rest mass of the electron, and γ_E is the relativistic factor associated with the energy E (in keV). For the results shown in the figures of this paper, $f(E, \alpha)$ has been assumed to be isotropic ($g(\alpha) = 1$), and A has been chosen such that $\Phi_E = 10^8$ el cm^{-2} s^{-1} sr^{-1} keV^{-1} for $E = 1$ keV for the case when $n = 4$. This Φ_E value is typical of the flux levels outside and just inside the plasmapause during geomagnetically disturbed times [*Schield and Frank,* 1970; *Anderson,* 1976] and was the reference flux level used in some of the previous work [*Inan et al.,* 1978, 1982; *Chang and Inan,* 1983; *Chang et al.,* 1983]. Although Φ_E is a highly variable quantity, we have chosen to present our results with the assumption that Φ_E is constant with L. For any realistic variation of Φ_E as a function of L, the precipitated flux values can be obtained from the results given by proper scaling. The implication of possible anisotropic distributions and variation of Φ_E will be discussed for different cases.

As the wave packet propagates up the field line, a fresh distribution of particles continually enters its leading edge. For example, at a time $t = \tau$ when the wave front is at latitude λ, a distribution of particles represented by (2) will encounter the wave packet. However, only a portion of these particles in a limited range of energy and a narrow range of pitch angle near the edge of the loss cone are scattered into the loss cone after the interaction. After taking into account the arrival times at the precipitation region and the contribution to the energy flux of different particles, a precipitated energy flux rate in erg cm^{-2} s^{-2}, denoted by $h(t, \tau)$, can be obtained. This $h(t, \tau)d\tau$ is then the precipitated energy flux at the precipitation region versus time t due to those particles that meet the leading edge of the propagating wave packet between times $t = \tau - \frac{1}{2}d\tau$ and $t = \tau + \frac{1}{2}d\tau$. Thus $h(t, \tau)$ is equivalent to the response at time t due to an external excitation applied to a system at time τ. The total system response, or the total precipitated energy flux as a function of time due to all downcoming particles that encounter the wave packet at different latitudes and times, is then the integral of $h(t, \tau)d\tau$. In other words,

$$r(t) = \int_0^\infty h(t, \tau)d\tau \tag{3}$$

where $r(t)$ is the precipitated energy flux at the precipitation region as a function of time after the wave injection.

In our model the full distribution of particles (2) is simulated by a large number of test particles. Using the cyclotron resonance condition (1) as a criterion, the ranges in energy and pitch angle of the particles that could be scattered into the loss cone are determined for each time τ when a new distribution of particles is introduced to meet the wave packet. Test particles in these ranges are then passed one by one through the integration of the equations of motion in which the relative motion between the particle and the wave packet is monitored. We have used the relativistic equations of motion as given by *Chang and Inan* [1983] so that the scattering of those higher-energy particles (i.e., $E > 50$ keV) can be correctly evaluated. After this computation, the energy and equatorial pitch angle of each scattered particle is known, and the perturbed distribution function is obtained. Consequently, the electrons that are scattered into the loss cone are summed to give the response $h(t, \tau)$ corresponding to the time τ.

This procedure for computing $r(t)$ is identical to that used in previous work and is described in detail by *Inan et al.* [1982]. In Figure 1 we give a typical example of the result. The top panel shows the precipitated energy flux versus time at the wave injection site for the case of a 0.4-s pulse at a frequency of 6.83 kHz and equatorial wave intensity 5 pT propagating along the $L = 4$ magnetic field line. The result given is for a diffusive eqilibrium model and an equatorial cold plasma density $n_{eq} = 400$ el/cm^3. The energetic particle distribution is given by (2) with $g(\alpha) = 1$

(isotropic), $n = 6$, and $\Phi_E = 10^8$ el cm^{-2} s^{-1} sr^{-1} keV^{-1} for $E = 1$ keV.

In calculating $h(t, \tau)$ for a given τ, only a limited range of particle energies will contribute to the energy flux. For different particle energies the arrival times are different, and we can therefore plot an energy versus time curve for each τ. The lower panel of Figure 1 gives such energy versus time curves for sample τ values corresponding to latitudes of the leading edge of the wave pulse ranging from $\lambda = -16°$ (the curve to the extreme left) to $\lambda = 44°$ in steps of 4°. The curves progress from lower left to lower right and then to upper right. The diagram thus gives the energy range of the downcoming precipitated flux as a function of time.

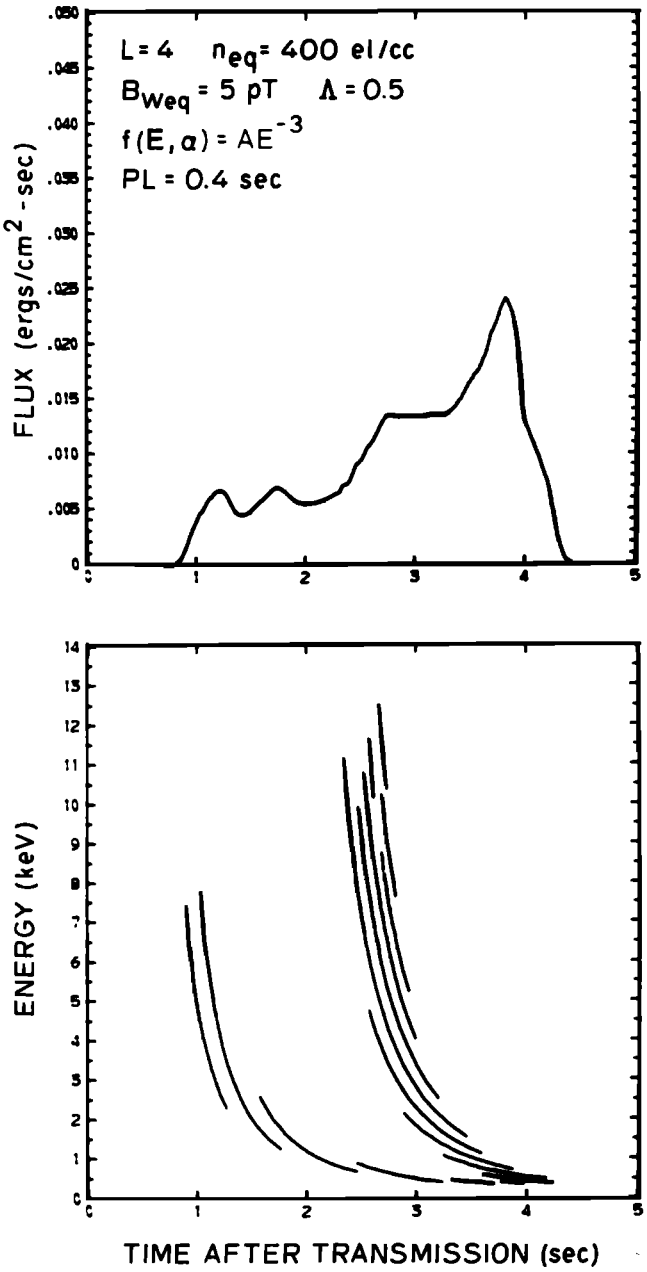

Fig. 1. Example showing the output of a model calculation. The upper panel shows the precipitated energy flux versus time after injection of the wave into the magnetosphere. The lower panel gives the energy of the particles that constitute the flux. Each separate segment represents the energy versus arrival time for one of the responses corresponding to one of the positions of the wave front. In this case the individual responses are computed for $\lambda = -16°$ to 44° with steps of 4°.

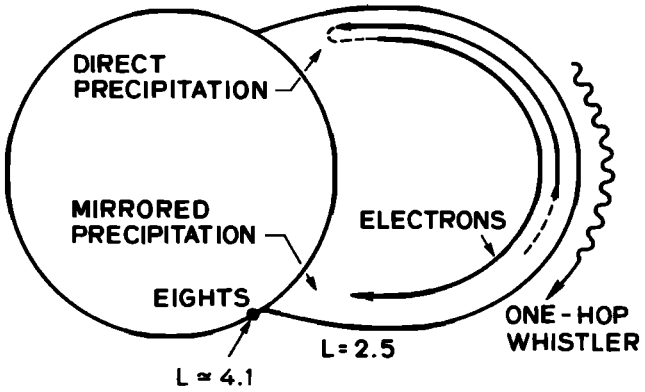

Fig. 2. Field line model showing the whistler-induced precipitation. The one-hop whistler could interact with north going trapped electrons near the equatorial region and cause precipitation of electrons in the northern hemisphere. Due to the asymmetry in the conjugate mirror altitudes, some resonant electrons can mirror in the north and be precipitated in the south near Eights Station.

3. The Case of Subionospheric VLF Perturbations

Helliwell et al. [1973] reported the observation of sudden changes in the amplitude of long-distance subionospheric VLF transmissions in association with whistlers. Sample observations at Eights Station in Antarctica of Station NSS (Annapolis, Maryland) on 22.3 kHz showed increases in signal strength that averaged 3 dB. Coincident with every rise a mid-latitude ($L \simeq 2.5$) whistler originating in the northern hemisphere was observed. To explain the association between the whistlers and the changes in VLF signal strength, it was suggested that the whistler precipitates energetic (30–300 keV) electrons into the D region. The resulting ionization then alters the properties of the earth-ionosphere waveguide. The mechanism of precipitation was thought to be pitch angle scattering of trapped electrons that resonate with the whistler wave near the magnetic equator.

Figure 2 illustrates the model employed in our calculations. The $L = 2.5$ field line with an equatorial electron density of 1800 el/cm^3 and a diffusive equilibrium model for the cold plasma is considered. These values correspond to the strongest whistler trace observed in the correlation events. The input signal in this case is a lightning stroke originating in the northern hemisphere, modeled as having entered the medium at 1000 km altitude at $t = 0$. The signal arrives at the southern conjugate point (near the longitude of Eights Station) as a one-hop whistler. The whistler interacts with north going trapped electrons near the equatorial region and can cause precipitation of some electrons into the loss cone. Due to the asymmetry in the conjugate mirror altitudes at this longitude [*Barish and Wiley,* 1970], some fraction of the resonant electrons would mirror in the north, and thus precipitation in both northern and southern hemispheres is possible.

Frequency-time formats of the whistler propagating at $L = 2.5$ are depicted in Figure 3. Only the 2–6 kHz portion is considered, being consistent with the observed

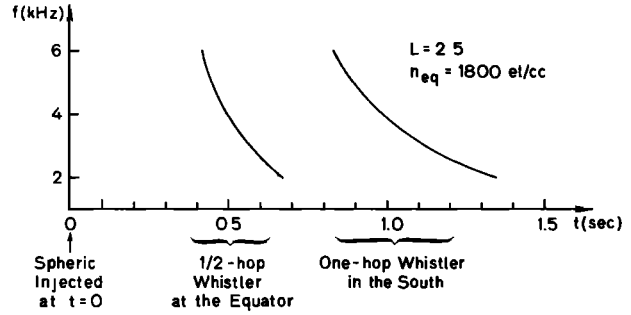

Fig. 3. The frequency-time formats of the whistler used in the computer model. Only the 2–6 kHz portion was considered, being consistent with the observed event. The duration of the signal observed at the equator (termed 1/2-hop whistler) is about 0.25 s, and that of the one-hop whistler received in the southern hemisphere is about 0.5 s.

event in that the strongest whistler signals appeared in this frequency band. The duration of the signal observed at the equator (termed half-hop whistler) is about 0.25 s and in the southern hemisphere (one-hop) is about 0.5 s.

The interaction between the whistler and a particle can be qualitatively understood by comparing the curves representing a specific particle's adiabatic parallel velocity $v_{\|}$ with the resonance velocity defined as

$$v_R = \frac{(\omega_H/\gamma - \omega)}{k} \tag{4}$$

plotted as functions of latitude along the field line. The particle is considered to be in resonance with the wave at a given point z along the field line at time t if locally $v_{\|} \simeq v_R$ at that time. The possible resonance locations between the particle and the wave are thus represented by the intersections of $v_{\|}$ and v_R curves.

The upper panel of Figure 4 shows a group of v_R curves and the $v_{\|}$ (dashed) curve of a particle with energy 187 keV and equatorial pitch angle 11.6° (equatorial half angle of the loss cone at $L = 2.5$ used in our calculation). Progressing in time from right to left, each v_R curve represents a case in which this particle enters the leading edge of the propagating whistler wave packet at a latitude (λ) corresponding to the left end point of that curve. The right end point corresponds to the latitude at which this 187-keV particle exits the wave packet. Between these two points, ω_H, k, and ω vary with respect to latitude due to the inhomogeneity of the medium and the frequency variation of the whistler wave. This panel shows that the given particle should undergo a resonant interaction with the wave near −15° latitude in the south. However, since the gradient of v_R versus latitude is large at that point, the particle moves out of the resonance region quickly, and the resulting equatorial pitch angle scattering $\Delta\alpha_{eq}$ in this case is less than 0.05°. The equatorial parallel velocity of this particle, i.e., 2×10^8 km/s (187 keV) has been used as the upper limit of the test particle distribution in this case. In other words, particles for which $\Delta\alpha_{eq} < 0.05°$ are assumed to be unaffected by the wave.

The lower panel shows the wave amplitude (B_w) variation experienced by the given particle within the wave packet corresponding to each v_R curve in the upper panel. The input signal is assumed to have a constant power spectral density uniformly distributed between 2 and 6 kHz, so that the wave intensities corresponding to lower frequencies are smaller due to the increased dispersion at lower frequencies. The total energy of the wave packet is taken to be that of a monochromatic pulse of duration 0.1 s and with equatorial wave intensity of 5 pT.

By examining the $v_{\|}$ and v_R curves for a particle with equatorial parallel velocity 1×10^8 km/s (31 keV) and equatorial pitch angle 11.6°, as was done in Figure 4, it was found that this particle does not interact with the given whistler. The v_R values in this case are higher than those in Figure 4, since the value of γ in equation (4) is smaller for the lower energy particles. This parallel velocity was used as the lower limit for the test particle distribution.

The calculated transient precipitated energy fluxes induced by this one-hop whistler wave packet are shown in Figure 5. Left panels show the direct precipitation fluxes in the north that would be observed after the injection of the impulsive spheric at $t = 0$, assuming that all precipitated

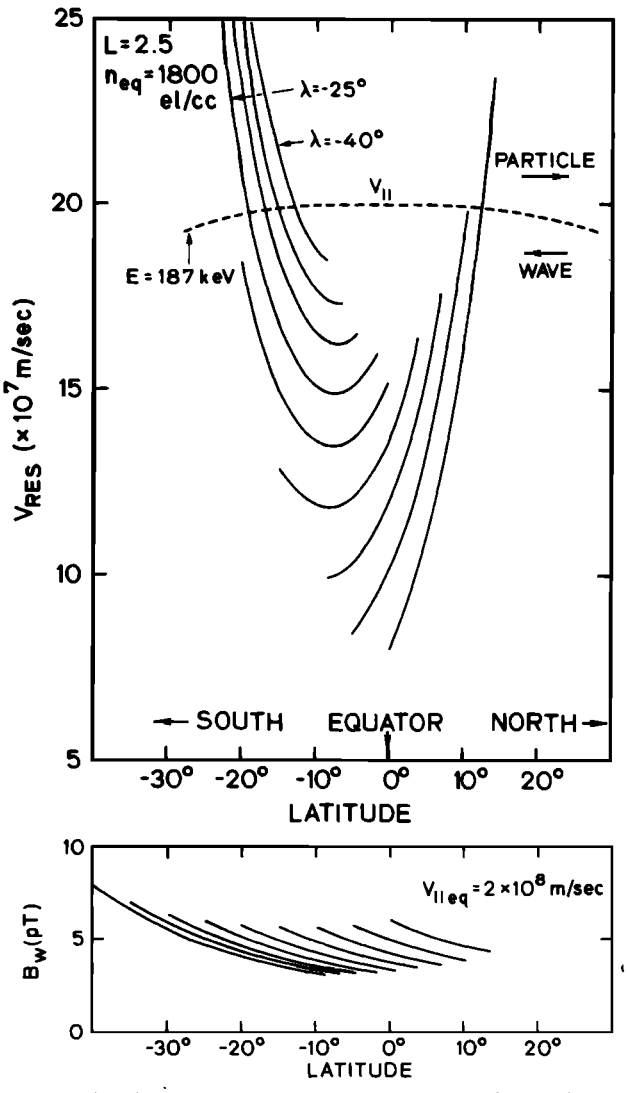

Fig. 4. (Top) A group of v_R curves and the $v_{\|}$ (dashed) curve of a particle with energy of 187 keV and pitch angle at the edge of the loss cone for the whistler case. Each v_R curve represents a case in which the particle enters the whistler front at a latitude corresponding to the left end of that curve. (Bottom) The wave amplitude variation experienced by the given particle within the wave packet corresponding to each v_R curve in the upper panel.

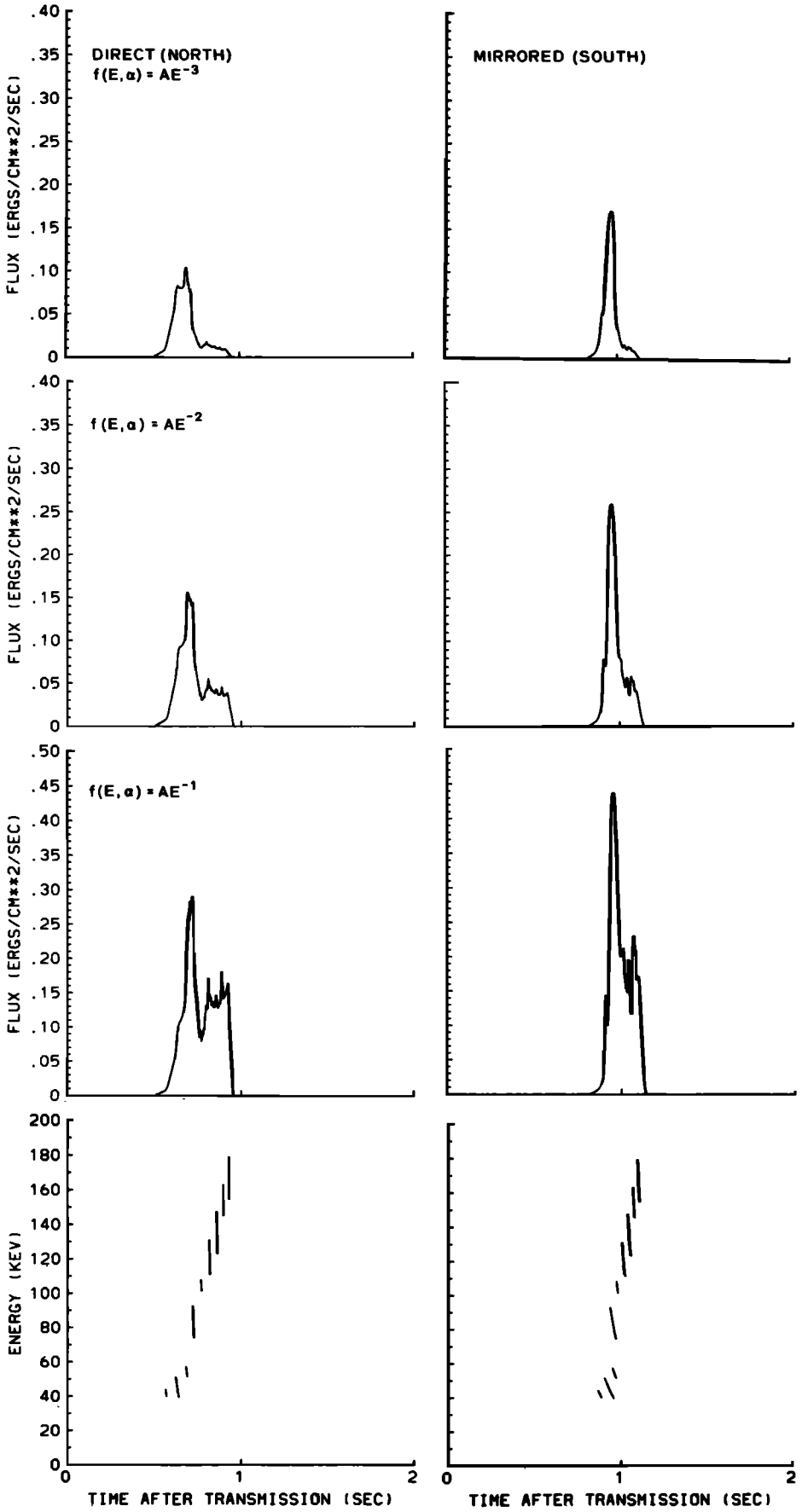

Fig. 5. (Left) The direct precipitation pulses in the north induced by the one-hop whistler given in Figure 3 for three different trapped distributions, assuming no mirrored particles. (Right) The corresponding mirrored precipitation pulses assuming that all precipitated particles mirror back. The bottom panels give the energy versus arrival time curves.

particles precipitate in the north without either backscattering or mirroring back southward. Three different variations with energy of the trapped particle distributions, i.e., $n = 6$, 4, and 2 in (2), are used. The differential energy spectrum Φ_E has been normalized to 1.78×10^6 el cm^{-2} s^{-1} sr^{-1} keV^{-1} for $E = 40$ keV, corresponding to $\Phi_E = 10^8$ el cm^{-2} s^{-1} sr^{-1} keV^{-1} for $E = 1$ keV when $n = 4$. For smaller n value, particles with higher energy play a more dominant role. The peak fluxes are due to those particles that interact strongly with the wave around $-10°$ latitude, since the v_R curves show obvious local minima there [*Chang et al.*, 1983]. The bottom panel gives the energy range of the precipitating particles at different times. One feature in this case is that the faster particles arrive later because they are scattered by the wave at later times.

The right panels of Figure 5 give the mirrored precipitation fluxes at the conjugate site assuming that all the scattered particles mirror in the north and precipitate in the south. The total precipitated energies in the direct and the mirrored precipitation cases for a given trapped distribution function are then the same. However, the peak flux of the mirrored case is at least 50% higher. This is due to the fact that the faster particles catch up with the slower particles, illustrating arrival time focusing of particles with different energies. The energy versus time diagrams indicate that the precipitated electrons are sufficiently energetic ($E > 40$ keV) to penetrate below the normal ionospheric reflecting height for VLF propagation [*Banks et al.*, 1974].

According to *Barish and Wiley* [1970], a mirror height of 100 km in the south corresponds to a conjugate mirror height of about 500 km along the $L = 2.5$ field for the longitude of Eights. This amounts to about 1.2° difference in the half angle of the equatorial loss cone α_{eq}^{lc} between the two hemispheres. It is found from individual test particle trajectories that for the wave intensity of $\simeq$5 pT used in our model, $\Delta\alpha_{eq} < 1.2°$. In fact, an equatorial wave intensity of >20 pT would be required for a 2–6 kHz signal at $L = 2.5$ to induce a $\Delta\alpha_{eq} > 1.2°$ on at least some of the interacting particles [*Inan et al.*, 1982]. Therefore most particles scattered in a single encounter with the wave would be outside the loss cone in the north and would thus mirror back to be deposited in the southern hemisphere. *Tolstoy et al.* [1982] used a propagation model to investigate the effect of localized ionospheric perturbations on the subionospheric VLF wave propagation for the case reported by *Helliwell et al.* [1973]. Their calculations suggest that two ionization regions, one very near the transmitter and another near the receiver, may be needed in order to obtain amplitude increases of >3 dB. It was suggested that the former was due to transmitter-induced electron precipitation. The one near the receiver would then be due to mirrored precipitation of the type indicated in Figure 5. From Figures 3 and 5 it is seen that the (mirrored) precipitation pulse (<0.3 s) has a shorter duration than the one-hop whistler packet ($\simeq$0.5 s), while their average arrival times are about the same.

The results of Figure 5 indicate that a precipitated flux of $>10^{-1}$ erg cm^{-2} s^{-1} could be obtained assuming $\Phi_E \simeq 10^6$ el cm^{-2} s^{-1} sr^{-1} keV^{-1} for $E = 40$ keV and a wave intensity of $\simeq$5 pT near the equatorial region. It should be noted that the calculated flux is directly proportional to Φ_E and thus can be scaled up or down according to different Φ_E values. Also, in the above calculation an isotropic distribution ($g(\alpha) = 1$) has been assumed. For an anisotropic distribution ($g(\alpha) \neq 1$ in (2)) peaked around $\alpha = 90°$, another scaling ($g(90°)/g(\alpha^{lc})$) is needed to account for the lower trapped flux level near the edge of the loss cone, since we use Φ_E at 90° pitch angle as the reference. Although Φ_E is an unknown factor in the present case, we know that the observation took place under relatively quiet geomagnetic conditions, and it is useful to estimate the possible precipitated flux level by using typical quiet time values for Φ_E. Under these conditions, according to *Lyons and Williams* [1975], $\Phi_E \simeq 10^5$ el cm^{-2} s^{-1} sr^{-1} keV^{-1} at 90° pitch angle and $g(90°)/g(\alpha^{lc}) \simeq 10$ for $E = 40$ keV and $L \simeq 3$. Then our computed flux level would be scaled down to $\sim 10^{-3}$ erg cm^{-2} s^{-1}. Moreover, when strong anisotropy in the vicinity of the loss cone rather than a sharp-edged loss cone is considered, a further reduction in flux by an order of magnitude might be necessary as discussed by *Inan et al.* [1982].

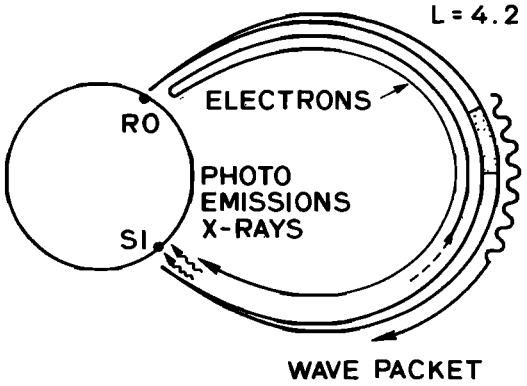

Fig. 6. Schematic showing that VLF emission signals triggered near the equator along the Siple-Roberval field line can scatter north going electrons which mirror above Roberval and then precipitate over Siple Station and cause X rays and photoemissions there.

4. THE X RAY CASE

The first one-to-one correlation between short bursts of bremsstrahlung X rays ($E > 30$ keV) and bursts of VLF discrete emissions was obtained on January 2, 1971, during balloon-borne measurements at Siple Station, Antarctica [*Rosenberg et al.*, 1971]. This correlation was interpreted in terms of a cyclotron resonance interaction in the vicinity of the geomagnetic equator and suggested that the wave-induced energetic electron precipitation would create the observed X rays. From an examination of the ground-based VLF recordings, it was determined that the waves led the arrival of the precipitating electrons by about 0.3–0.4 s.

It was found that every major burst of X rays was associated with VLF rising tones of duration $\simeq$0.5–3 s. The rising emissions were deduced to be triggered by whistlers from lightning discharges in the northern hemisphere. The triggering region was presumed to be near the geomagnetic equator on the downstream side for the particles. Two possible situations could cause precipitation of particles at Siple Station: a north going wave could scatter south going electrons into the loss cone and result in direct precipitation, while a south going wave could also scatter north going electrons which then mirror in the north and result in mirrored precipitation in the south. For the case in hand,

the mirrored precipitation was found to provide a better explanation than direct precipitation based on the analysis of wave and particle travel times. [*Rosenberg et al.*, 1971].

Figure 6 shows a schematic description of the reported correlation event of January 2, 1971. A south going wave packet of VLF emissions triggered near the equator scatters north going electrons which mirror above Roberval and precipitate above Siple Station, generating bremsstrahlung X rays. Such mirrored precipitation is possible due to the asymmetry in the conjugate mirror altitudes for the Roberval-Siple field line.

In our model calculation, a rising ramp with frequency varying from 2 to 4 kHz is injected onto the $L = 4.2$ field line above Roberval at 1000 km altitude at time $t = 0$, such that the signal received at Siple would be a rising ramp with duration of 0.5 s. To account for the triggering of the observed emissions near the equator, the wave intensity of the input signal is assumed to be zero in the northern hemisphere along the field line, while it is taken to be that corresponding to a 5-pT equatorial intensity in the region to the south of the equator. The mirrored transient precipitation energy flux above Siple is then obtained as a function of time after the injection of the input signal, assuming that all the scattered particles would mirror above Roberval.

The equatorial electron density n_{eq} on the $L = 4.2$ field line at the time of the observed correlation was estimated through whistler scaling to be 25 ± 12 el/cm^3. In this paper we compute the precipitated fluxes for $n_{eq} = 13$, 25, and 37 el/cm^3. Although the above estimation was based on a collisionless model (D. L. Carpenter, private communication, 1983), both diffusive equilibrium and collisionless models of the cold plasma distribution along the field line will be considered in the following.

Figure 7 shows the mirrored transient precipitation fluxes obtained by assuming $n_{eq} = 25$ el/cm^3 and the collisionless model. Left panels give the fluxes contributed by the range of energies $E > 20$ keV of particles scattered into the loss cone by the waves (2–4 kHz). Since the bursts of X rays that were correlated with the waves had energies of >30 keV and were mainly caused by electrons with energy of >60 keV [*Rosenberg et al.*, 1971; *Foster and Rosenberg*, 1976], it is interesting to examine the fluxes due only to particles with $E > 60$ keV. These are shown in the corresponding right-hand panels in Figure 7. Three different variations with energy of the trapped particle distribution, i.e., E^{-4}, E^{-3}, and E^{-2}, are considered, with the differential energy spectrum Φ_E normalized to 10^6 el cm^{-2} s^{-1} sr^{-1} keV^{-1} for $E = 60$ keV. As in the case of Figure 5, for $n = 4$ in (2) this corresponds to $\Phi_E = 10^8$ el cm^{-2} s^{-1} sr^{-1} keV^{-1} for $E = 1$ keV. The transient precipitation pulses on the left-hand panels are of longer duration due to the wider range in the downcoming electron energy as well as the greater travel times of the lower-energy electrons. For $n > 6$ the peak fluxes depend primarily on the lower-energy particles. However, the precipitation pulses obtained by considering only $E > 60$ keV are much narrower and show well-defined peaks. Note that the arrival time of the peak flux does not significantly depend on n in (2). This fact allows a more straightforward determination of the time lag between the X ray burst and the wave pulse. The energy versus arrival time curves for both cases are given in the bottom panels.

Note that the energy versus time curves given in the bottom panels of Figure 7 can also be compared with the data. *Foster and Rosenberg* [1976] cross-correlated the X ray data in two different energy ranges with the VLF wave data and showed that the differential arrival time of particles in the 30–68 keV and 68–143 keV ranges was about 0.1 s. The arrival time variation given in Figure 7 is in rough agreement with this measured value as well as the calculated variation shown by *Foster and Rosenberg* [1976].

In order to see the dependence of the result on the cold plasma models and n_{eq}, we show the results of six different cases in Figure 8. Left panels are for the collisionless (R-4) model, while right panels are for the diffusive equilibrium model. In each panel the arrival time at the southern hemisphere of the leading edge ($f = 2$ kHz) of the wave packet is indicated by an arrow on the time axis.

The travel time along the $L = 4.2$ field line for a signal at 4 kHz is smaller than that at 2 kHz for each case. Therefore the input wave packet duration has been set equal to 0.5 s plus the difference Δt_{PL} between the travel times of 4-kHz and 2-kHz waves, such that the duration of the received wave packet in the south is 0.5 s for each case. Since Δt_{PL} is generally larger for the R-4 model, for the same n_{eq} the input wave duration for the R-4 model is larger than that for the DE model. This accounts for the higher peak in the R-4 model case; the input energy, set to be proportional to the input wave duration, is larger. Note that the equatorial wave intensity is the same in both cases.

In Figure 9 is plotted the time lag between the peak of the flux and the arrival of the wave front as a function of n_{eq} for both the diffusive equilibrium and collisionless models. The shaded area indicates the observed time lag in the experiment. Our theoretical results based on the collisionless model and $n_{eq} \simeq 25$ el/cm^3 are in good agreement with the observations.

The results of Figures 7 and 8 are obtained based on the assumption that all the precipitated electrons mirror back in the north. They show that a peak flux of >0.1 erg cm^{-2} s^{-1} could be obtained if the equatorial wave intensity is of the order of 5 pT and if Φ_E is $\simeq 10^6$ el cm^{-2} s^{-1} sr^{-1} keV^{-1} for $E = 60$ keV. Note again that this calculation is obtained by assuming an isotropic distribution, or $g(\alpha) = 1$ in (2). Since this X ray case was observed during a gradual-commencement magnetic storm, the assumption of isotropy would be more reasonable than in the case discussed in section 3. On the Siple-Roberval field line a mirror height of 100 km in the south corresponds to a conjugate mirror height of 280 km [*Barish and Wiley*, 1970]. Using this, our test particle calculations show that more than 95% of the precipitated particles mirror at the northern end, since $\Delta\alpha_{eq}$ experienced by most of these high-energy ($E > 60$ keV) particles is smaller than the difference (about 0.2°) in the equatorial half angle of the two loss cones. The above assumption that all electrons mirror back is then a good approximation.

5. THE PHOTOEMISSION CASE

One-to-one correlations were observed at $L \simeq 4.2$ between bursts of VLF noise in the $\simeq$2 to 4 kHz range and optical emissions at $\lambda \simeq 4278$ Å at Siple Station in the austral winter of 1977 [*Helliwell et al.*, 1980]. The correlated VLF wave activity usually consisted of clusters of discrete rising tones or chorus. In the case of July 24, 1977, all of

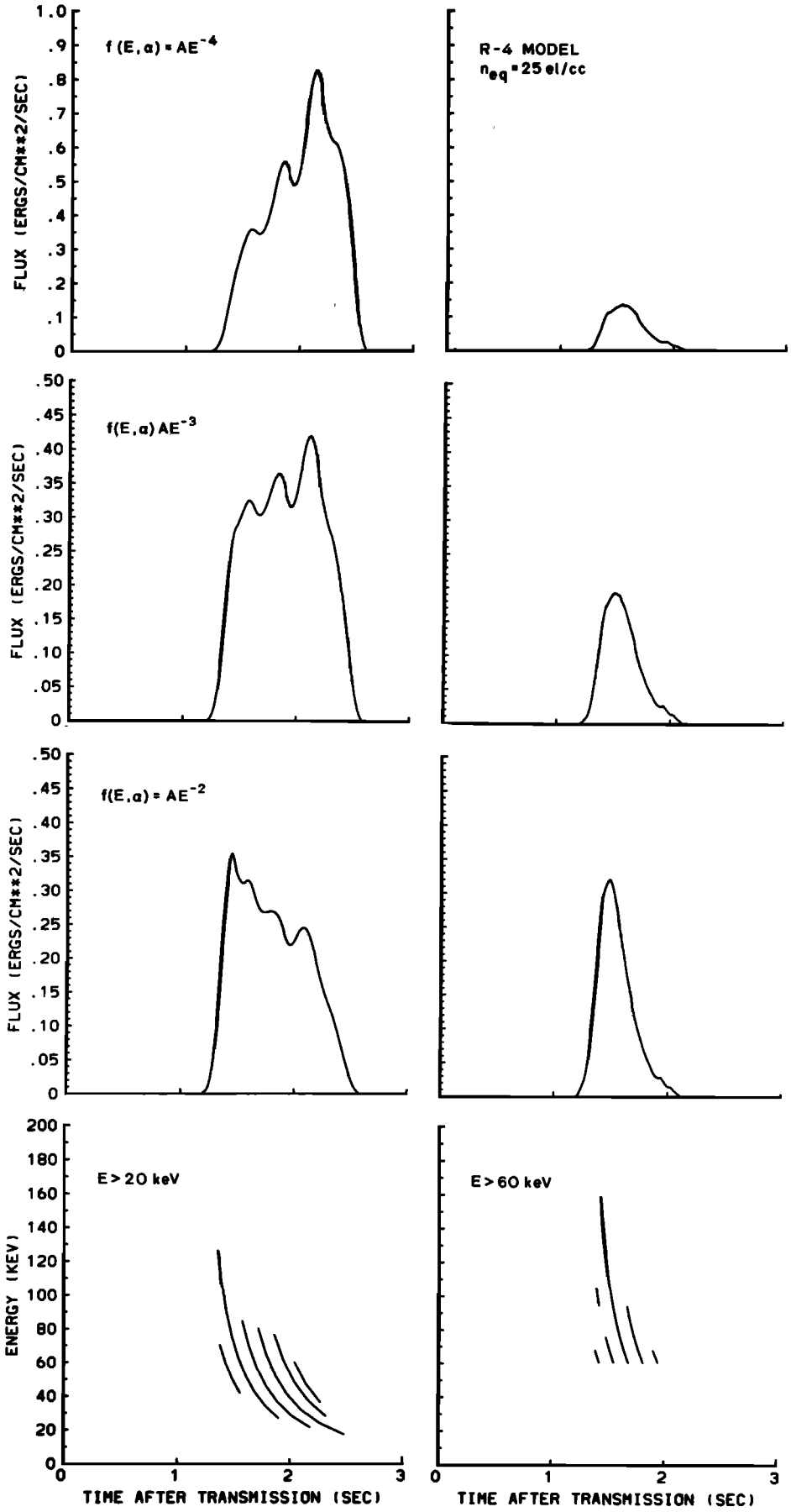

Fig. 7. The mirrored transient precipitation fluxes obtained by assuming $n_{eq} = 25$ el/cm^3 and the collisionless model for the X ray case. Left hand panels give the fluxes obtained by the whole range of energies ($E > 20$ keV) of particles scattered into the loss cone by the waves, while right hand panels show the fluxes contributed from particles with $E > 60$ keV. Three different trapped particle distributions are considered with Φ_E normalized to 10^6 el cm^{-2} s^{-1} sr^{-1} keV^{-1} for $E = 60$ keV.

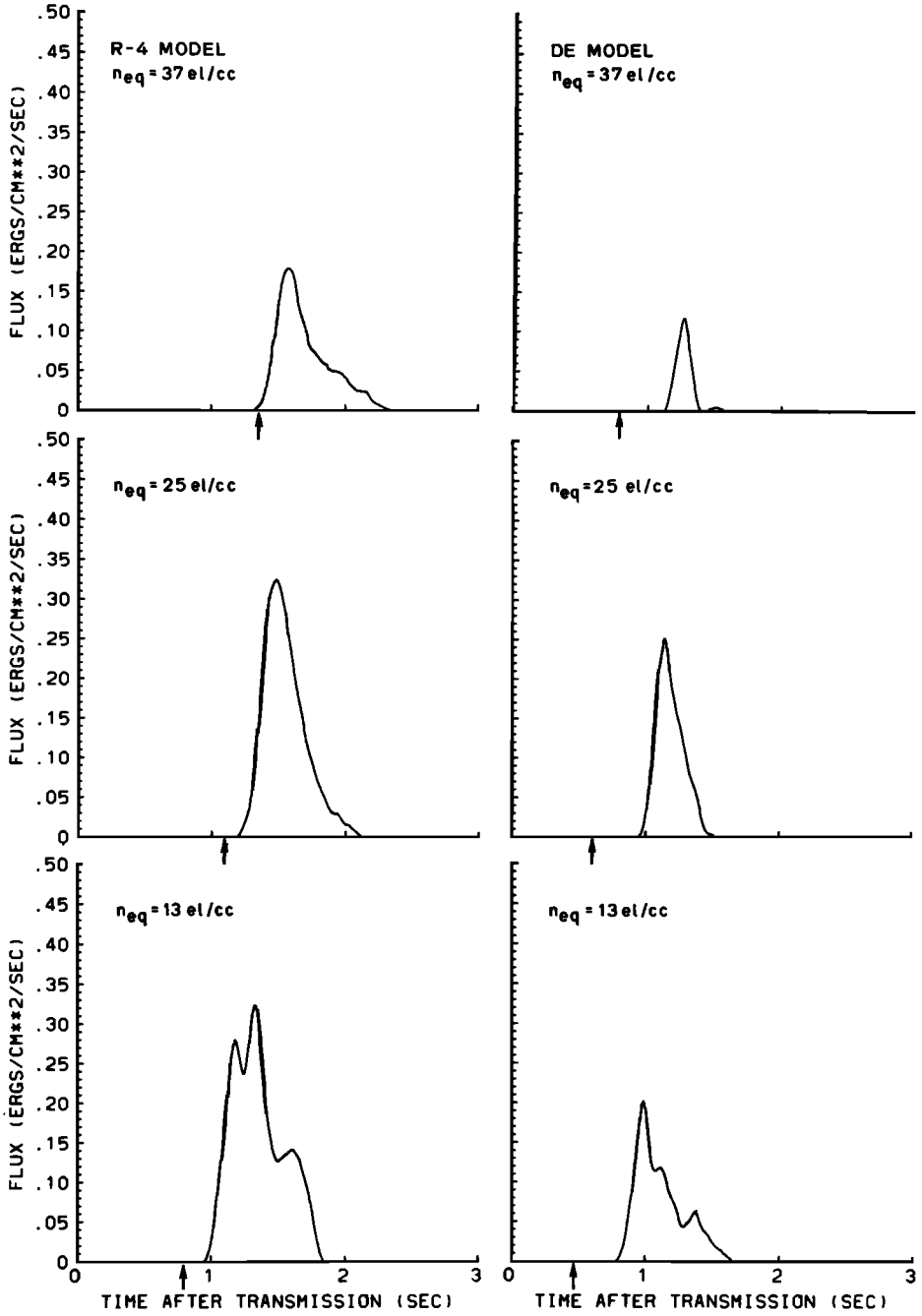

Fig. 8. The mirrored precipitation fluxes computed for the X ray case. Left-hand panels are for the collisionless model while right-hand panels are for the diffusive equilibrium model. Three different n_{eq} values are used. In each panel the arrival time of the wave front is marked by an arrow along the time axis.

the correlated wave events involved whistlers and whistler-triggered emissions. In this particular case, the length of the wave train observed at Siple was estimated to be about 1.2 s, and the observed photometer pulse was found to occupy the time interval 2.6–4.3 s after the occurrence ($t = 0$) of the lightning-generated spheric observed near Roberval. For propagation at $L \simeq 4.2$, the equatorial cold plasma density and the equatorial wave magnetic field were deduced to be $n_{eq} = 100$ el/cm^3 and $B_w \approx 8$ pT, respectively.

The field line model for this photometer case is the same as that depicted in Figure 6. As in the X ray case discussed in section 4, both direct and mirrored precipitations are candidates that may account for the optical emissions over Siple Station. The possible importance of direct precipitation is suggested by the fact that at the top of the ionosphere the field intensity of the north going wave was estimated to be only 2 dB less than that of the south-going wave [*Helliwell et al.*, 1980], thus indicating efficient echoing of the wave back and forth between hemispheres.

In the following we calculate both the direct and the mirrored precipitation fluxes induced by the wave event corresponding to the case of July 24, 1977. The signal received at Siple is modeled as a rising ramp with duration of 1.2 s and with frequency varying from 2 to 4 kHz. For the mir-

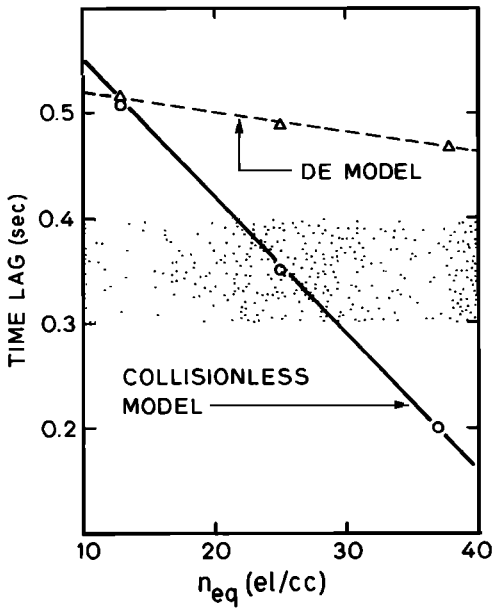

Fig. 9. Time lag between the peak of the flux and the arrival of the wave (marked by an arrow in Figure 5) as a function of n_{eq} for the diffusive equilibrium and collisionless models. The shaded area indicates the observed time lag.

rored case in which the wave is south going, the wave intensity in the northern hemisphere along the field line is taken to be zero to account for the fact that the whistler-induced emission was probably generated near the equator, while it is taken to be 8 pT to the south of the equator in accordance with the estimation from the data. However, for the case of the north-going wave that causes direct precipitation, the wave intensity is taken to be 8 pT on both sides of the equator. A diffusive equilibrium model is used for the cold plasma distribution along the $L = 4.2$ field line with $n_{eq} = 100$ el/cm^3.

As mentioned in the introduction, in order to account for all the particles that could contribute to the observed photoemission, a wide range of particle energies need to be considered. To see the effect of the fall-off in energy of the trapped particle distribution function, we normalize $f(E, \alpha)$ such that $\Phi_E = 10^8$ el cm^{-2} s^{-1} sr^{-1} keV^{-1} for $E = 1$ keV and for different values of n in (2).

Upper panels of Figure 10 show the temporal variations of the computed precipitated fluxes for $n = 6$ in (2). Note that $t = 0$ corresponds to the instant when the lightning impulse occurred near the field line above Roberval. Lower panels show the corresponding energy versus arrival time curves. The pitch angle resolution in this case is $\Delta\alpha = 0.05°$ so that particle energies up to $\simeq$180 keV are included.

Using half magnitude of the peak flux as a criterion, the precipitation pulses are found to occupy the intervals $t = 1.9$–4.2 s and $t = 2.5$–4.0 s for the mirrored and direct precipitation cases, respectively. Compared with the data ($t = 2.6$–4.3 s), the direct case gives a slightly better fit. The fact that the direct precipitation pulse does rise abruptly near $t \simeq 2.5$ s further favors this interpretation. However, the significant overlap in time between the two responses suggests that both the mirrored and the direct precipitation may be contributing to the observed flux. Due to the mirror height difference between the ends of the Siple-Roberval field line, our calculations show that only 75% of the precipitated particles contribute to the mirrored precipitation. Thus the absolute flux level of the mirrored case in Figure 10 should be reduced by this factor, since we assumed that all precipitated particles mirrored back at that point. Note here that since the photoemission is caused by a wide range of energies including relatively low ones, the percentage of particles which mirror in the north in this case is expected to be lower than that of the X ray case, since the lower energy particles experience larger $\Delta\alpha_{eq}$ and thus scatter into the loss cone in the north without mirroring back. In summary, the model calculations suggest that the observed photoemission could be due to a combination of both mirrored and direct precipitating particles, with more than half of the contribution being due to the direct precipitation.

The calculated flux level is a function of B_w and the assumed trapped particle distribution. In the present case, B_w has been inferred from the data. The assumed particle distribution is then the main factor that determines the computed flux level. For a case in which the particle energy covers a wide range as in this one, the value of n in (2) is the key parameter that affects the relative contributions to the flux of high- and low-energy particles. For fixed n, the energy flux level is proportional to Φ_E. In Figure 11, we plot the peak flux level versus n with Φ_E as a parameter for the case of direct precipitation. The shaded area indicates the range ($\simeq$0.04–0.1 erg cm^{-2} s^{-1}) of the precipitated energy fluxes inferred from the photometric data [*Helliwell et al.*, 1980]. If $\Phi_E = 10^8$ el cm^{-2} s^{-1} sr^{-1} keV^{-1} then $n \approx 5.5$–6 would fit the observed downcoming flux. However, if Φ_E is reduced by 2 orders, n would be less than 4. Figure 11 implies that under typical flux levels of $\Phi_E = 10^6$–10^8 el cm^{-2} s^{-1} sr^{-1} keV^{-1} [*Lyons and Williams*, 1975] the value of n would fall in the range of $\simeq$3.5–6 based on the observed precipitating fluxes. To the best of our knowledge, this constitutes a new method of remotely estimating the decrease with energy of the trapped particle distribution in the magnetosphere. Our estimated value of $n \simeq 3.5$–6 is in substantial agreement with published direct measurements [*Schield and Frank*, 1970]. Since the above results are obtained by assuming $g(\alpha) = 1$ in (2), inclusion of any anisotropy would reduce the calculated fluxes as discussed at the end of section 3 and therefore would result in smaller estimated n values, or a less steep distribution with respect to E.

6. Summary and Conclusions

We have applied a test particle computer model to compute the transient evolution of the precipitated particle fluxes induced by VLF waves that have been reported to be correlated with energetic electron precipitation events. The relationship between the downcoming flux levels and the possible trapped energetic electron distributions can be obtained for each case. Our model employs exact equations of motion for the gyroresonant wave-particle interaction, including relativistic effects, so that the wave-induced perturbations in individual particle trajectories can be correctly computed for particle energies up to hundreds of keV.

Three different events representing three different methods of detecting the ionospheric effects of precipitating electron fluxes, i.e., the observations of perturbations of subionospheric VLF signals, bremsstrahlung X rays, and photoemissions, have been studied in this paper. In the case of subionospheric VLF perturbations [*Helliwell et al.*, 1973], it was concluded that mirrored precipitation could have caused D region enhancements near the receiver be-

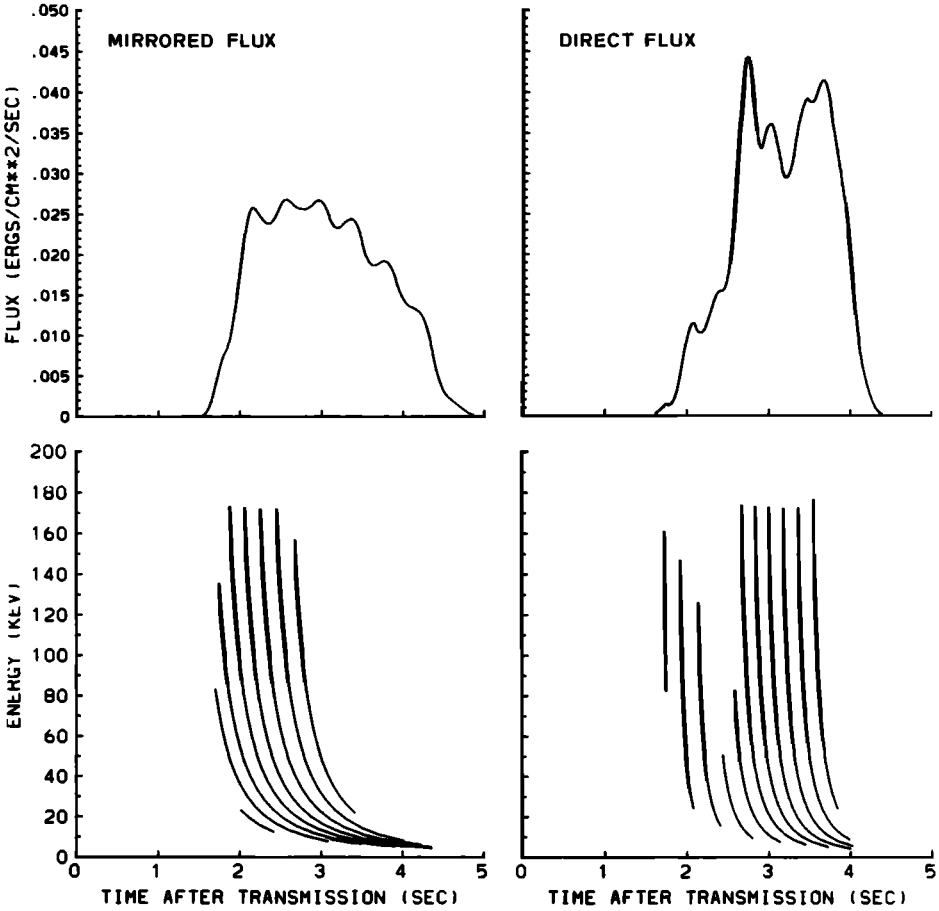

Fig. 10. Precipitation fluxes and energy curves calculated for the photometer case; $n = 6$ in equation (2) is assumed. Left-hand panels show the mirrored mode induced by the south going wave. Right-hand panels show the direct mode caused by the north going wave.

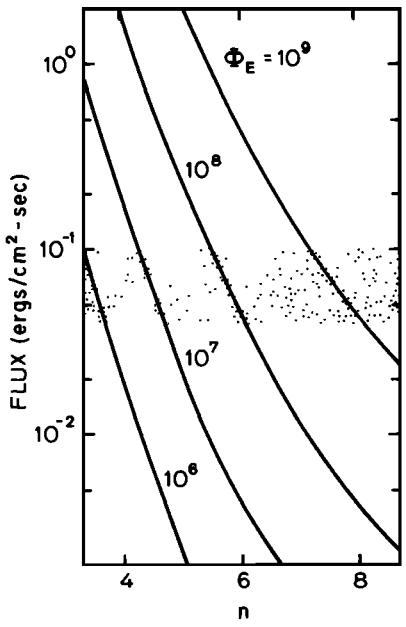

Fig. 11. Peak flux level versus n in equation (2) with Φ_E as a parameter for the case of direct precipitation for the photometer case. The shaded area indicates the range of the precipitated energy fluxes inferred from the data.

cause of the significant mirror height difference (100 km versus 500 km) for the given longitude and field line. In the case of X ray observations [*Rosenberg et al.*, 1971], it was shown that the computed time lag between the wave packet and precipitation pulse was consistent with the cold plasma model deduced from the observed data. Finally, in a case of photometric observations [*Helliwell et al.*, 1980] in which the observed data involved a wider range of particle energies, it was shown that the value of n in equation (2) can be estimated from the observed data. For the case in hand, n was found to be in the range of $\simeq$3.5 to 6 for typical values of trapped particle fluxes.

We have compared the predictions of an existing theoretical computer-based model of the coherent wave-induced precipitation of radiation belt particles with ground based observations of the ionospheric effects of such precipitation. Our results demonstrate that the model can be useful for interpreting the observed experimental results. Furthermore, the model results and observations, used together, provide a basis for additional diagnostics of the various parameters of the cold and energetic particle distributions in the magnetosphere. The successful application of the model to three different experimental situations indicates its versatility; an obvious potential application is in planning of future experiments aimed at detecting wave-induced particle precipitation and its ionospheric effects.

Acknowledgments. We wish to acknowledge the many discussions we have held with our colleagues at Stanford and especially with R. A. Helliwell. This research was supported by the National Aeronautics and Space Administration under grant NGL-05-020-008 and by the National Science Foundation under grant ATM-80-18248. The computer calculations were made using the CRAY-1 computers of the National Center for Atmospheric Research (NCAR) in Boulder, Colorado. Our use of this facility was made possible by a Computer Resources grant from NCAR.

The Editor thanks J. C. Siren and T. J. Rosenberg for their assistance in evaluating this manuscript.

REFERENCES

Anderson, R. R., Wave particle interactions in the evening magnetosphere during geomagnetically disturbed periods, Ph.D. thesis, Univ. of Iowa, Iowa City, 1976.

Banks, P. M., C. R. Chappell, and A F. Nagy, A new model for the interaction of auroral electrons with the atmosphere: Spectral degradation, backscatter, optical emission, and ionization, *J. Geophys. Res., 79,* 1495, 1974.

Barish, F. D., and R. E. Wiley, World contours of conjugate mirror locations, *J. Geophys. Res., 75,* 6342, 1970.

Carpenter, D. L., and J. W. LaBelle, A study of whistlers correlated with bursts of electron precipitation near $L = 2$, *J. Geophys. Res., 87,* 4427, 1982.

Chang, H. C., and U. S. Inan, Quasi-relativistic electron precipitation due to interactions with coherent VLF waves in the magnetosphere, *J. Geophys. Res., 88,* 318, 1983.

Chang, H. C., U. S. Inan, and T. F. Bell, Energetic electron precipitation due to gyroresonant interactions in the magnetosphere involving coherent VLF waves with slowly varying frequency, *J. Geophys. Res., 88,* 7037, 1983.

Dingle, B., and D. L. Carpenter, Electron precipitation induced by VLF noise bursts at the plasmapause and detected at conjugate ground stations, *J. Geophys. Res., 86,* 4597, 1981.

Doolittle, J. H., Modification of the ionosphere by VLF wave-induced electron precipitation, Ph.D. thesis, Radiosci. Lab., Stanford Electron. Labs., Stanford Univ., Stanford, Calif., 1982.

Doolittle, J. H., and D. L. Carpenter, Photometric evidence of electron precipitation induced by first hop whistlers, *Geophys. Res. Lett., 10,* 611, 1983.

Foster, J. C., and T. J. Rosenberg, Electron precipitation and VLF emissions associated with cyclotron resonance interactions near the plasmapause, *J. Geophys. Res., 81,* 2183, 1976.

Helliwell, R. A., J. P. Katsufrakis, and M. L. Trimpi, Whistler-induced amplitude perturbation in VLF propagation, *J. Geophys. Res., 78,* 4679, 1973.

Helliwell, R. A., S. B. Mende, J. H. Doolittle, W. C. Armstrong, and D. L. Carpenter, Correlations between λ4278 optical emissions and VLF wave events observed at $L \sim 4$ in the Antarctic, *J. Geophys. Res., 85,* 3376, 1980.

Inan, U. S., T. F. Bell, and R. A. Helliwell, Nonlinear pitch angle scattering of energetic electrons by coherent VLF waves in the magnetosphere, *J. Geophys. Res., 83,* 3235, 1978.

Inan, U. S., T. F. Bell, and H. C. Chang, Particle precipitation induced by short-duration VLF waves in the magnetosphere, *J. Geophys. Res., 87,* 6243, 1982.

Lohrey, B., and A. B. Kaiser, Whistler-induced anomalies in VLF propagation, *J. Geophys. Res., 84,* 5722, 1979.

Lyons, L. R., and D. J. Williams, The quiet time structure of energetic (35–560 keV) radiation belt electrons, *J. Geophys. Res., 80,* 943, 1975.

Rosenberg, T. J., R. A. Helliwell, and J. P. Katsufrakis, Electron precipitation associated with discrete very-low-frequency emissions, *J. Geophys. Res., 76,* 8445, 1971.

Rosenberg, T. J., J. C. Siren, D. L. Matthews, K. Marthinsen, J. A. Holtet, A. Egeland, D. L. Carpenter, and R. A. Helliwell, Conjugacy of electron microbursts and VLF chorus, *J. Geophys. Res., 86,* 5819, 1981.

Schield, M. A., and L. A. Frank, Electron observations between the inner edge of the plasma sheet and the plasmasphere, *J. Geophys. Res., 75,* 5401, 1970.

Tolstoy, A., T. J. Rosenberg, and D. L. Carpenter, The influence of localized precipitation-induced *D*-region ionization enhancements on subionospheric VLF propagation, *Geophys. Res. Lett., 9*(5), 563, 1982.

H. C. Chang and U. S. Inan, Space, Telecommunications and Radioscience Laboratory, Stanford University, Stanford, CA 94305.

(Received February 28, 1983;
revised July 12, 1983;
accepted July 20, 1983.)